R. & M. No. 3702

R. & M. No. 3702

MINISTRY OF DEFENCE (PROCUREMENT EXECUTIVE)

AERONAUTICAL RESEARCH COUNCIL
REPORTS AND MEMORANDA

Effects of Reynolds Number and Frequency Parameter on Control-Surface Buzz at High Subsonic Speeds

By Y. NAKAMURA and L. WOODGATE

Aerodynamics Division, N.P.L.

LONDON: HER MAJESTY'S STATIONERY OFFICE

1972

PRICE 70p NET

Effects of Reynolds Number and Frequency Parameter on Control-Surface Buzz at High Subsonic Speeds

By Y. NAKAMURA* and L. WOODGATE

Reports and Memoranda No. 3702†
February, 1970

Summary.

Stiffness and damping hinge-moment derivatives have been measured on a two-dimensional aerofoil-flap combination model by a free-oscillation technique. The experiments were conducted in the N.P.L. 18 in × 14 in (0·46 m × 0·36 m) tunnel where it is possible to vary the stagnation pressure and hence the Reynolds number and frequency parameter. To separate the effects of Reynolds number and frequency, flaps of different inertias were used. Measurements were made only in the range of Mach number where control surface buzz oscillations started spontaneously. A method of controlling the flap oscillation was developed which depended on the use of fine air jets issuing from the model surface just forward of the flap. Although changes in Reynolds number produced only small changes in the derivatives, these changes were larger for low values of frequency parameter; the magnitude of the derivatives tended to increase with Reynolds number. The effect of frequency parameters was larger; the values of the limit cycle amplitude and both derivatives decreased numerically with increasing frequency.

LIST OF CONTENTS

* Guest worker at N.P.L. during 1965.
† Replaces A.R.C. Report 31 897.

1. Introduction.

This investigation on a two-dimensional aerofoil with a trailing-edge flap is related to a programme of work at the N.P.L. concerned with the measurement of unsteady aerodynamic hinge moments. Lambourne[1] has shown that there exists at least three types of buzz instability in two-dimensional transonic flow, each associated with a particular flow regime. The present work is concerned with the first type of buzz, which occurs at subsonic speeds and is associated with shock waves ahead of the control surface. Lambourne has defined the various non-dimensional parameters which can influence buzz, and it was expected that amongst these, the frequency parameter would be of particular importance, since it was already known that the amplitude of the flap oscillation at the limit cycle of buzz decreases with the increase of the angular stiffness of the flap about its hinge. On the other hand, the oscillations for this type of buzz were believed to be closely associated with shock-induced separation of the boundary layer; differences were already known to exist between buzz characteristics with turbulent and laminar boundary layers. The primary purpose of the present experiment was to obtain information on the effects of Reynolds number on the buzz characteristics.

Since it is only a turbulent boundary layer that is of interest in practical flying conditions, the investigation was restricted to the cases where transition occurred ahead of the shock. To obtain a variation in Reynolds number a variable-density tunnel was used. Attention was restricted to the range of Mach number within which buzz occurs. As was expected with this type of buzz, oscillations started spontaneously. The amplitude was allowed to grow until the natural limit was reached and the unsteady hinge moment and the amplitude of the limit cycle were deduced from records of the time-history of the growing oscillations.

Because the angular stiffness of the flap about its hinge was mainly aerodynamic, a change in the stagnation pressure resulted in a considerable change in the frequency of oscillation. In other words, the variation in the stagnation pressure led to changes both in Reynolds number and in frequency parameter. By using flaps of different inertias, the effects of Reynolds number and frequency parameter could be separated and thus the measurements also provided information on the effect of frequency parameter.

An opportunity was taken to make high speed cine records of the shock waves and the boundary layer during buzz.

Detailed discussions on the mechanism of the onset of buzz based on the present experimental results and the results of the flow visualization are given in a separate paper by the first author[2].

2. Description of Model and Apparatus.

The 18 in × 14 in (0·46 m × 0·36 m) variable-density transonic wind-tunnel was used for the present experiment. As shown in Figs. 1 and 2 the model was a two-dimensional aerofoil-flap combination with a 10 per cent thick RAE 102 section. The model spanned the working section of the tunnel. The aerofoil was rigidly supported by the tunnel walls at a fixed incidence of 4 degrees. Five flaps of the same profile but with different values of moment of inertia about the hinge were used. Each flap could be attached to

the main aerofoil by means of a spring hinge consisting of a thin steel strip that ensured a low system damping. Although the design hinge-line coincided with the centre-line of the spring, observation showed that the actual hinge-line during oscillation was very close to the forward clamped end of the spring. However, the effect of this offset on the buzz characteristics is considered to be small. Data concerning the aerofoil and the flap are given in Table 1.

The leading edge of the aerofoil was roughened with a band of carborundum grains (grain size 0·08 mm) to provide a turbulent boundary layer which was more representative of flight conditions. The flap movement had to start from a suitable stationary position so that the rate of growth of the amplitude of oscillation could be measured. As the oscillations were self-excited some provision had to be made to prevent them from starting before uniform flow had been established in the tunnel. This was achieved by the use of fine air jets issuing from the upper surface of the aerofoil ahead of the hinge line. Apparatus was designed to allow the air jets to be switched off extremely rapidly, thus allowing the oscillation to start under the required aerodynamic conditions. This method proved quite effective in suppressing the oscillation for a limited speed range above the critical Mach number for buzz.

As is shown in Fig. 2, air-jets with a supply ranging from 28×10^4 N/m^2 to 69×10^4 N/m^2, depending on the stagnation pressure used, were injected into the separated flow through a row of small holes of 0·5 mm in diameter in the upper surface of the aerofoil. These holes were drilled vertically at 0·543 chord behind the leading edge and at intervals of 3·2 mm in the spanwise direction. The air was supplied through a brass tube which was inserted in the aerofoil and had holes corresponding to those in the aerofoil. The air could only be injected when the holes in the tube and the aerofoil were lined up; thus by rotating the tube to offset the positions of the holes, the injection of the air could be rapidly cut off, the time required being about 2 or 3 milliseconds.

The movement of the flap was monitored by an optical tracking instrument (an "Optron 680 Tracker") situated outside the working section. The electrical output of this instrument was proportional to the displacement of the flap. By applying this signal to the vertical plates of a cathode-ray oscilloscope and triggering the oscilloscope time base from the lever which controlled the air jets, the time history of the flap movement was displayed on the oscilloscope and recorded photographically.

3. Range of Investigation and Method of Measurement.

Tests were made at $M = 0{\cdot}78$, 0·79, 0·80, 0·81 and 0·82. At $M = 0{\cdot}82$ the air jet control was not so effective and sometimes failed to suppress buzz. This is possibly because the shock wave was then located downstream of the air jets. The stagnation pressure was varied from 10×10^4 N/m^2 (31 in Hg) to 20×10^4 N/m^2 (60 in Hg). The corresponding values of Reynolds number, based on the aerofoil chord, ranged from $1{\cdot}6 \times 10^6$ to $3{\cdot}2 \times 10^6$. (Table 2).

The method of determining the aerodynamic hinge-moment derivatives from the frequency and the rate of growth of the oscillation assumes a linear system. It was found that the frequency was practically constant for all amplitudes but the rate of growth was exponential only up to three degrees approximately. Larger amplitudes were therefore not analysed. A considerable amount of scatter was found in the experimental results due possibly to small fluctuations in the tunnel flow. Four transients were therefore recorded for each condition and the mean values were used in the calculations. The method of data reduction is given in the Appendix. Measurements outside the buzz Mach number region were not made because of the difficulty of deflecting the flap without introducing large distortions.

4. Experimental Results.

With increasing speed, buzz occurred spontaneously at a Mach number slightly below 0·78. This critical Mach number was found to be the same for all flap inertias and for all Reynolds numbers tested. Under these conditions, a shock wave was present on the upper surface and caused separation of the boundary layer; no shock wave was present on the lower surface except when the flap had a large upward deflection.

Direct shadowgraph pictures (Figs. 3a and 3b) show the flow patterns around the aerofoil with and

without air jets at $M = 0{\cdot}77$, which was just below the critical Mach number. Fig. 3c shows the flow at $M = 0{\cdot}78$ with air jets on, but for which, buzz would have occurred. Although the precise role played by air jets in suppressing buzz is not known, it seems likely that their influence on the separated flow upsets an interaction between shock wave and flap movement.

Two records of the growth of the flap oscillation obtained for the same conditions are given in Fig. 4, and the corresponding curves, plotted in Fig. 5, show the growth of amplitude against cycle of oscillation. It is clear from these graphs that the amplitude of oscillation increased exponentially with time for amplitudes less than 3 degrees. Some of the numerical values of buzz frequency, log increment and limit cycle amplitude for flap B are presented in Table 3.

The results for limit cycle amplitude and aerodynamic unsteady hinge moment are given in Table 4 and shown in Figs. 6 to 9 for each of the Mach numbers for which measurements were made, with the exception of $M = 0{\cdot}82$, for which the variations of the amplitude with cycle of oscillation were not exponential even for small amplitudes. The discussion will be mainly concerned with the results for $M = 0{\cdot}78$ and $0{\cdot}80$, which are considered to be most representative.

4.1. Limit Cycle Amplitude.

It is obvious from Figs. 6 to 9 that frequency has a large effect on the limit cycle amplitude; the amplitude decreases with increasing frequency parameter. It is difficult to determine the effect of Reynolds number on the limit cycle amplitude, firstly because of the scatter of the experimental data and secondly because of the unknown effects of structural damping. Although the use of the spring hinge ensured a minimal structural damping, it would be expected to make an increasing and significant contribution to the in-quadrature forces as the stagnation pressure was reduced. In general it would appear that an increase in Reynolds number leads to an increase in the limit cycle amplitude. At the higher values of the frequency parameter the effect is generally small but at the lower values it can be considerable.

4.2. Unsteady Hinge-Moment Derivatives.

Both the stiffness and the damping derivatives decrease numerically with increasing frequency (Figs. 6 to 9). The variation of the damping derivative with frequency is similar to that of the limit cycle amplitude in that they both tend to zero at about the same frequency parameter. In general it will be seen that an increase of Reynolds number leads to an increase in the magnitude of the hinge moment. The effect is larger on the damping derivative than on the stiffness derivative, and for both, it is greater for the lower values of the frequency parameter.

The variation in the oscillatory aerodynamic hinge-moment with frequency can also be seen by considering the change in the vector corresponding to the resultant of the in-phase and in-quadrature hinge moments. Fig. 10 shows, for each of two Mach numbers and atmospheric stagnation pressure, the locus of the tip of the hinge-moment vector with the variation of frequency parameter. These values were obtained by interpolation from Figs. 6 and 8. The points from the present experiment all correspond to negative damping and consequently lie above the horizontal axis. Also shown in Fig. 10 are some unpublished results obtained by K. C. Wight on an aerofoil similar to the present model but with a 0·23 m (9 in) chord, in the N.P.L. 36 in × 14 in (0·91 m × 0·36 m) tunnel at a Mach number of 0·75. Under these conditions, self-excited oscillations did not occur; the measurements being obtained by a forced-oscillation technique. The values shown in the diagram have been interpolated from Wight's results, to correspond with the frequency parameters of the present experimental results in Fig. 10; they are below the horizontal axis, corresponding to positive damping, and display the normal variation for a condition without shock-wave boundary-layer interaction. In comparison with the present results they show comparatively little variation of the in-phase component with frequency parameter.

5. Concluding Remarks.

The effects of Reynolds number changes between $1{\cdot}6 \times 10^6$ and $3{\cdot}2 \times 10^6$ are small but not negligible. The effects become larger for low values of frequency parameter and for these the magnitudes of the hinge moment derivatives tend to increase with Reynolds number. The effects of frequency parameter are

larger; the limit cycle amplitude and both derivatives decrease numerically with increasing frequency. Furthermore, the limit cycle amplitude and the damping derivative both tend to zero at approximately the same frequency.

6. Acknowledgements.

The authors wish to thank Mr. N. C. Lambourne and Mr. H. H. Pearcey for their advice and helpful comments on this work; Mr. K. C. Wight for providing unpublished experimental data, Mr. P. T. Taylor and Mr. W. W. Smith for the design and construction of the apparatus, and Mr. V. G. Quincey and Mr. R. Wood for their assistance in conducting the experiments.

LIST OF SYMBOLS

C_F	Flap chord
f	Frequency of oscillation
H_0	Stagnation Pressure
H	Hinge moment
$H_\beta, H_{\dot\beta}, H_{\ddot\beta}$	Hinge moment derivatives
$h_\beta, h_{\dot\beta}$	Non-dimensional forms of H_β, $H_{\dot\beta}$
I	Moment of inertia
s	Span of Model
M	Mach number
V	Wind speed
t	Time
β	Angular displacement of flap
$\beta_{\max}$	Amplitude of limit cycle
δ	Logarithmic increment
λ	Exponent for growing oscillations
μ	Apparatus damping
$v=\frac{\omega CF}{V}$	Frequency parameter
ρ	Air density
σ	Elastic stiffness of flap hinge
$\omega=2\pi f$	Angular velocity
R	Reynolds number

REFERENCES

No.	*Author(s)*	*Title, etc.*
1	N. C. Lambourne	Control surface buzz. A.R.C. R. & M. No. 3364, 1962.
2	Y. Nakamura	Some contributions on a control-surface buzz at high subsonic speeds. Journal of Aircraft, Vol. 5, No. 2, p. 118, 1968.

APPENDIX

If it is assumed that the system is linear, it follows that

$$I\ddot{\beta}+\mu\dot{\beta}+\sigma\beta=H_{\beta}B+H_{\dot{\beta}}\dot{\beta}+H_{\ddot{\beta}}\ddot{\beta}\,. \tag{A.1}$$

A solution for equation (1) is

$$\beta(t)=\beta_0 \exp{(\lambda+i\omega)t}$$

which gives,

$$I(\lambda+i\omega)^2+\mu(\lambda=i\omega)+\sigma=H_{\beta}+H_{\dot{\beta}}(\lambda+i\omega)+H_{\ddot{\beta}}(\lambda+i\omega)^2 \tag{A.2}$$

or

$$I(\lambda^2-\omega^2)\,\mu\lambda+\sigma=H_{\beta}+H_{\dot{\beta}}\,\lambda+H_{\ddot{\beta}}(\lambda^2-\omega^2) \tag{A.3}$$

and

$$I.2\,\lambda+\mu=H_{\dot{\beta}}+H_{\ddot{\beta}}\,.\;2\,\lambda\,. \tag{A.4}$$

If it is assumed that $I >> H_{\ddot{\beta}}$, equations (A.3) and (A.4) become

$$I(\lambda^2-\omega^2)+\mu\lambda+\sigma=H_{\beta}+H_{\dot{\beta}}\,\lambda \tag{A.5}$$

or

$$2\,\lambda\,I+\mu=H_{\dot{\beta}}\,. \tag{A.6}$$

Substituting from equation (A.6) into equation (A.5) gives

$$I(\lambda^2-\omega^2)+\mu\lambda+\sigma=H_{\beta}+\lambda(2\,\lambda\,I+\mu)$$

or

$$\sigma-(\lambda^2+\omega^2)\,I=H_{\beta}\,. \tag{A.7}$$

Equations (A.6) and (A.7) can then be used to determine the aerodynamic derivatives from the measured quantities.

The analysis of the records of the growth of the oscillations gave values of the oscillation frequency, f and logarithmic increment δ from which values of ω and λ were obtained as follows,

$$\omega=2\pi f$$

and

$$\lambda=\delta f\,.$$

The structural stiffness σ, was measured by a separate static experiment and values for I and μ were determined from still-air oscillatory experiments. For still-air equations (A.6) and (A.7) become

$$2\lambda_0 I+\mu=0$$

and

$$\sigma-(\lambda_0{}^2+\omega_0{}^2)I=0\,.$$

The hinge moments are presented in non-dimensional form. The relationship between the dimensional and non-dimensional values are as follows

$$h_{\beta}=\frac{H_{\beta}}{lV^2 C_F{}^2 s}$$

and

$$h_{\dot{\beta}}=\frac{H_{\dot{\beta}}}{lV^2 C_F{}^3 s}\,.$$

TABLE 1

Model Details.

Aerofoil section	RAE 102
Thickness to chord ratio	0·10
Position of maximum thickness	0·356 from leading edge
Span	0·356 m (14 in)
Chord	0·114 m (4·5 in)
Flap to aerofoil chord ratio	0·25

Flaps	A	B	C	D*	E*
$I \times 10^7$ kg.m^2	333·00	201·70	89·83	136·50	63·20
f_0 Hz	30·90	45·18	64·50	51·90	74·40
δ_0	−0·15	−0·054	−0·074	−0·055	−0·057

* Flaps D & E were of a preliminary design and were not tested over the full range of Mach numbers and stagnation pressure.

TABLE 2

Range of Mach Number, Stagnation Pressure and Reynolds Number used in the Experiments.

Mach number $M = 0{\cdot}78, 0{\cdot}79, 0{\cdot}80, 0{\cdot}81.$

Stagnation Pressure $H_0 \times 10^{-4}$ (N/m^2)	10·5	13·5	16·9	20·3
Reynolds number based of chord ($R \times 10^{-6}$)	1·6	2·1	2·6	3·2

TABLE 3

Typical Values of Frequency, Logarithmic and Limit Cycle Amplitude obtained from Photographic Records.

Flap B

$Ho = 10{\cdot}5 \times 10^4$ N/m^2

M	$f(Hz)$	δ	β_{max} (deg)
0·78	103·5	0·452	13·7
0·79	105·6	0·642	14·7
0·80	106·5	0·700	14·5
0·81	107·7	0·605	13·6

$Ho = 20{\cdot}3 \times 10^4$ N/m^2

M	$f(Hz)$	δ	β_{max} (deg)
0·78	131·5	0·780	13·2
0·79	132·0	0·958	13·6
0·80	133·0	1·10	13·2
0·81	133·0	1·02	12·3

TABLE 4

Results of the Experiments for the Various Flaps.

Flap A

$Ho = 10{\cdot}5 \times 10^4$ N/m^2, $R = 1{\cdot}6 \times 10^6$

M	v	$-h_\beta$	$+h_{\dot\beta}$	β_{max}
0·78	0·0610	0·470	1·37	12·1
0·79	0·0612	0·481	1·54	12·6
0·80	0·0616	0·494	1·63	12·6
0·81	0·0614	0·495	0·838	12·1

$Ho = 13{\cdot}5 \times 10^4$ N/m^2, $R = 2{\cdot}1 \times 10^6$

M	v	$-h_\beta$	$+h_{\dot\beta}$	β_{max}
0·78	0·0685	0·478	1·93	14·5
0·79	0·0704	0·512	2·02	16·4
0·80	0·0710	0·525	1·92	16·9
0·81	0·0702	0·518	1·32	16·9

$Ho = 16{\cdot}9 \times 10^4$ N/m^2, $R = 2{\cdot}6 \times 10^6$

M	v	$-h_\beta$	$+h_{\dot\beta}$	β_{max}
0·78	0·0770	0·493	1·70	16·9
0·79	0·0777	0·505	2·14	17·9
0·80	0·0788	0·525	1·85	18·5
0·81	0·0778	0·518	1·89	17·4

Flap B

$Ho = 10{\cdot}5 \times 10^4$ N/m^2, $R = 1{\cdot}6 \times 10^6$

M	v	$-h_\beta$	$+h_{\dot\beta}$	β_{max}
0·78	0·0745	0·396	0·965	13·7
0·79	0·0752	0·408	1·39	14·7
0·80	0·0750	0·412	1·51	14·5
0·81	0·0748	0·416	1·32	13·6

$Ho = 13{\cdot}5 \times 10^4$ N/m^2, $R = 2{\cdot}1 \times 10^6$

M	v	$-h_\beta$	$+h_{\dot\beta}$	β_{max}
0·78	0·0816	0·382	1·20	14·9
0·79	0·0820	0·392	1·56	14·9
0·80	0·0820	0·395	1·47	14·5
0·81	0·0815	0·397	1·53	13·2

$Ho = 16{\cdot}9 \times 10^4$ N/m^2, $R = 2{\cdot}6 \times 10^6$

M	v	$-h_\beta$	$+h_{\dot\beta}$	β_{max}
0·78	0·0890	0·374	1·10	14·5
0·79	0·0890	0·380	1·58	14·0
0·80	0·0890	0·384	1·51	13·6
0·81	0·0880	0·378	1·31	12·3

$Ho = 20{\cdot}3 \times 10^4$ N/m^2, $R = 3{\cdot}2 \times 10^6$

M	v	$-h_\beta$	$+h_{\dot\beta}$	β_{max}
0·78	0·0947	0·362	1·08	13·2
0·79	0·0941	0·358	1·32	13·6
0·80	0·0935	0·358	1·54	13·2
0·81	0·0925	0·354	1·39	12·3

TABLE 4 (*contd.*)

Flap C

$Ho = 10{\cdot}5 \times 10^4$ N/m^2, $R = 1{\cdot}6 \times 10^6$

M	v	$-h_\beta$	$+h_{\dot\beta}$	β_{max}
0·78	0·1025	0·328	0·585	8·3
0·79	0·1014	0·325	1·025	9·5
0·80	0·1025	0·336	1·060	9·9
0·81	0·1025	0·342	1·050	9·5

$Ho = 13{\cdot}5 \times 10^4$ N/m^2, $R = 2{\cdot}1 \times 10^6$

M	v	$-h_\beta$	$+h_{\dot\beta}$	β_{max}
0·78	0·110	0·303	0·158	4·55
0·79	0·109	0·301	0·706	7·6
0·80	0·1096	0·308	0·984	8·0
0·81	0·1095	0·312	1·082	7·6

$Ho = 16{\cdot}9 \times 10^4$ N/m^2, $R = 2{\cdot}6 \times 10^6$

M	v	$-h_\beta$	$+h_{\dot\beta}$	β_{max}
0·78	0·1190	0·292	0·350	4·17
0·79	0·1186	0·295	0·733	6·45
0·80	0·120	0·304	0·730	6·83
0·81	0·120	0·309	0·820	6·45

$Ho = 20{\cdot}3 \times 10^4$ N/m^2, $R = 3{\cdot}2 \times 10^6$

M	v	$-h_\beta$	$+h_{\dot\beta}$	β_{max}
0·78	0·1252	0·274	0·282	3·42
0·79	0·1258	0·281	0·652	5·30
0·80	0·1255	0·282	0·755	5·70
0·81	0·1295	0·308	0·795	5·30

Flap D

$Ho = 10{\cdot}5 \times 10^4$ N/m^2, $R = 1{\cdot}6 \times 10^6$

M	v	$-h_\beta$	$+h_{\dot\beta}$	β_{max}
0·78	0·0900	0·400	0·750	9·7
0·79	0·0888	0·395	1·045	9·7
0·80	0·0884	0·406	1·300	10·6
0·81	0·0882	0·398	1·170	10·1

$Ho = 13{\cdot}5 \times 10^4$ N/m^2, $R = 2{\cdot}6 \times 10^6$

M	v	$-h_\beta$	$+h_{\dot\beta}$	β_{max}
0·78	0·1042	0·347	0·543	
0·79	0·1033	0·344	0·890	8·2
0·80	0·1035	0·347	1·026	8·6
0·81	0·1040	0·356	1·005	8·4

Flap E

$Ho = 10{\cdot}5 \times 10^4$ N/m^2, $R = 1{\cdot}6 \times 10^6$

M	v	$-h_\beta$	$+h_{\dot\beta}$	β_{max}
0·78	0·1118	0·267	0·288	5·75
0·79	0·1120	0·273	0·608	7·15
0·80	0·1130	0·282	0·686	7·85
0·81	0·1130	0·290	0·660	7·45

$Ho = 13{\cdot}5 \times 10^4$ N/m^2, $R = 2{\cdot}6 \times 10^6$

M	v	$-h_\beta$	$+h_{\dot\beta}$	β_{max}
0·79	0·126	0·221	0·158	2·76
0·80	0·128	0·235	0·259	3·90
0·81	0·136	0·274	0·363	3·90

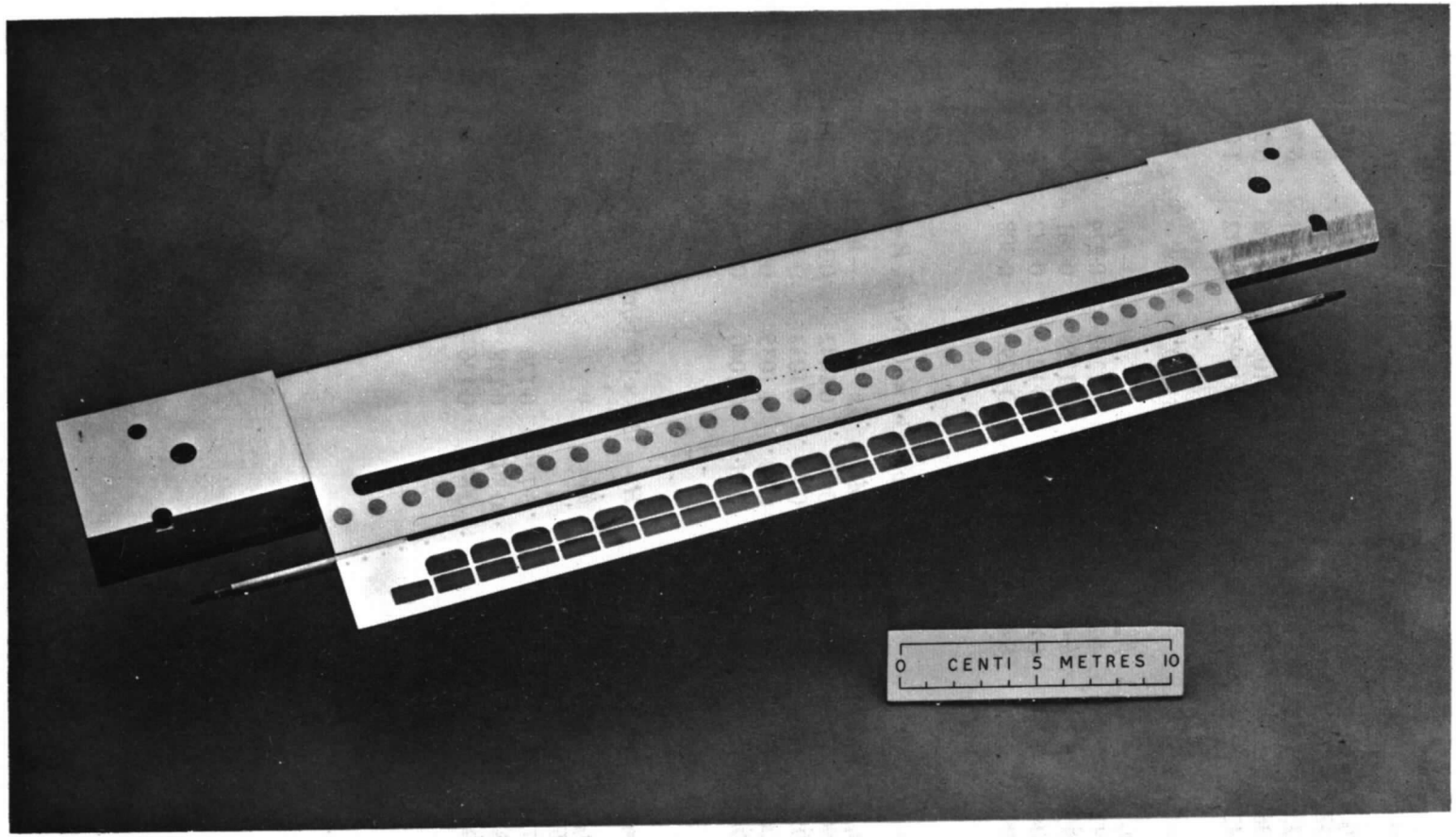

FIG. 1. Aerofoil-flap combination model.

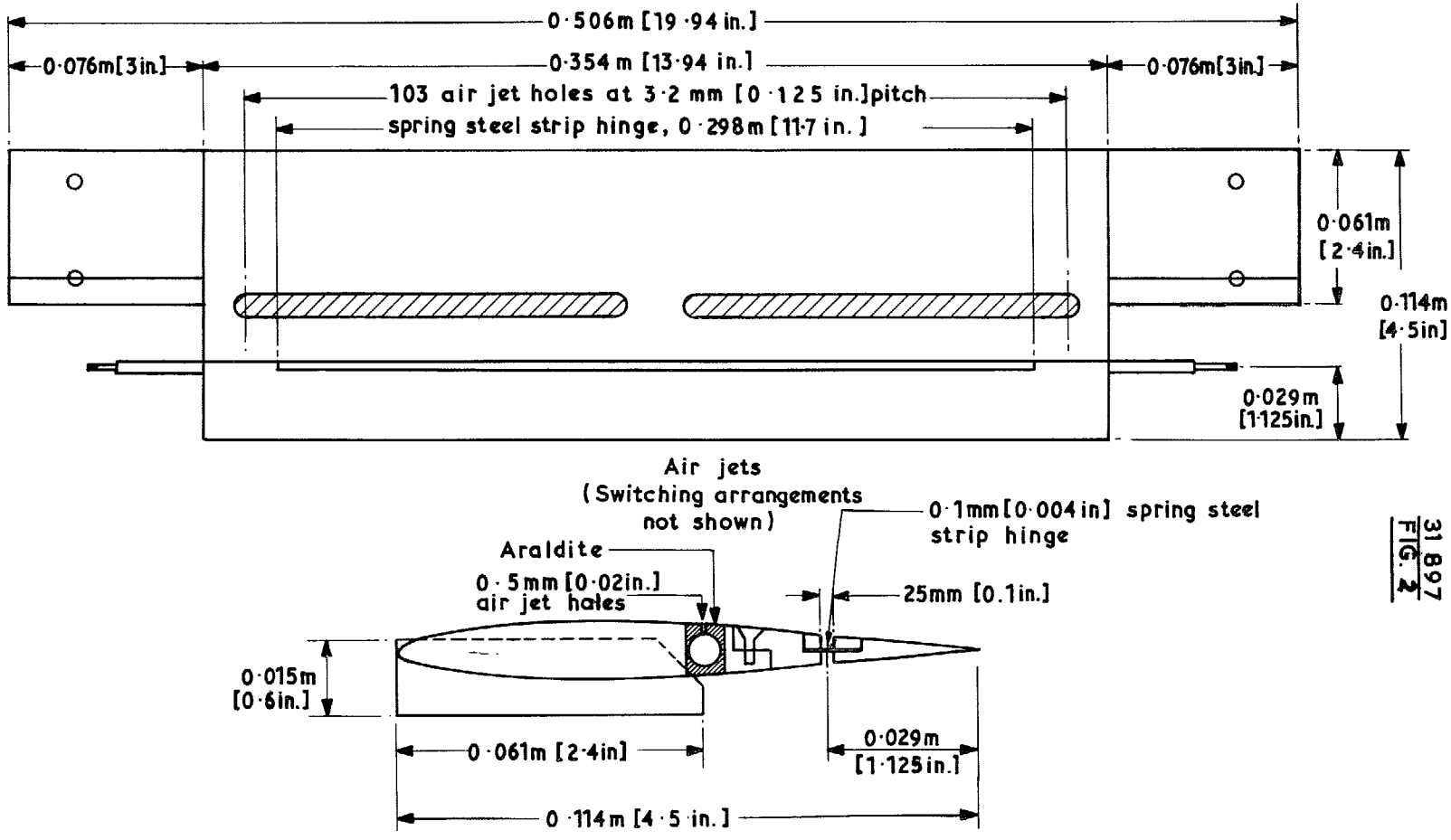

FIG. 2. Details of model.

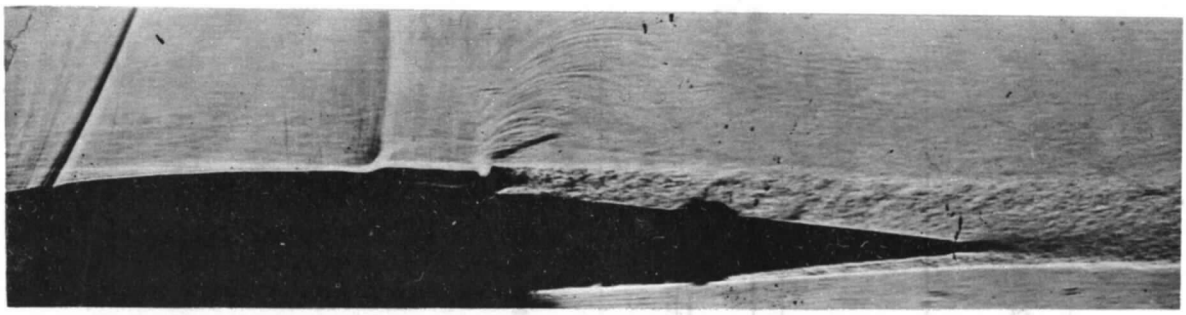

FIG. 3a. Direct shadowgraph. Air jets on. $M=0{\cdot}77$.

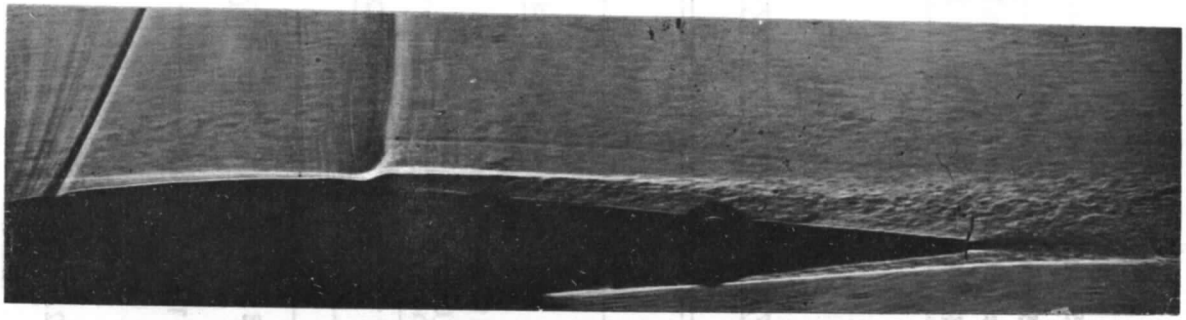

FIG. 3b. Direct shadowgraph. Air jets off. $M=0{\cdot}77$.

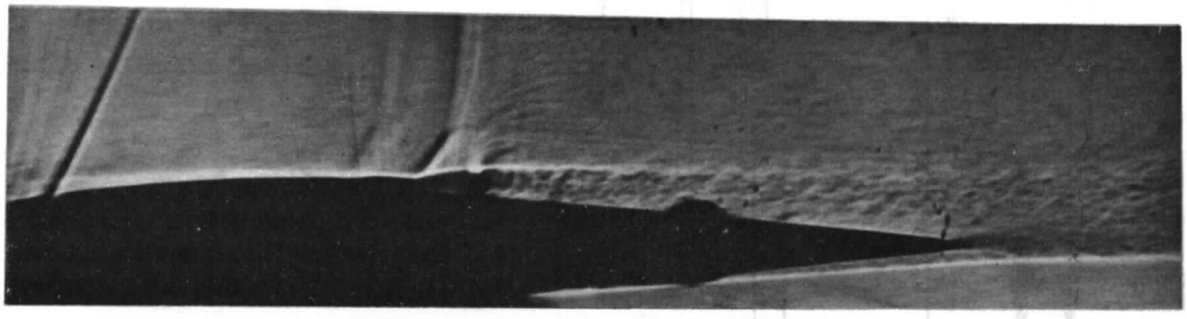

FIG. 3c. Direct shadowgraph. Air jets on. $M=0{\cdot}78$.

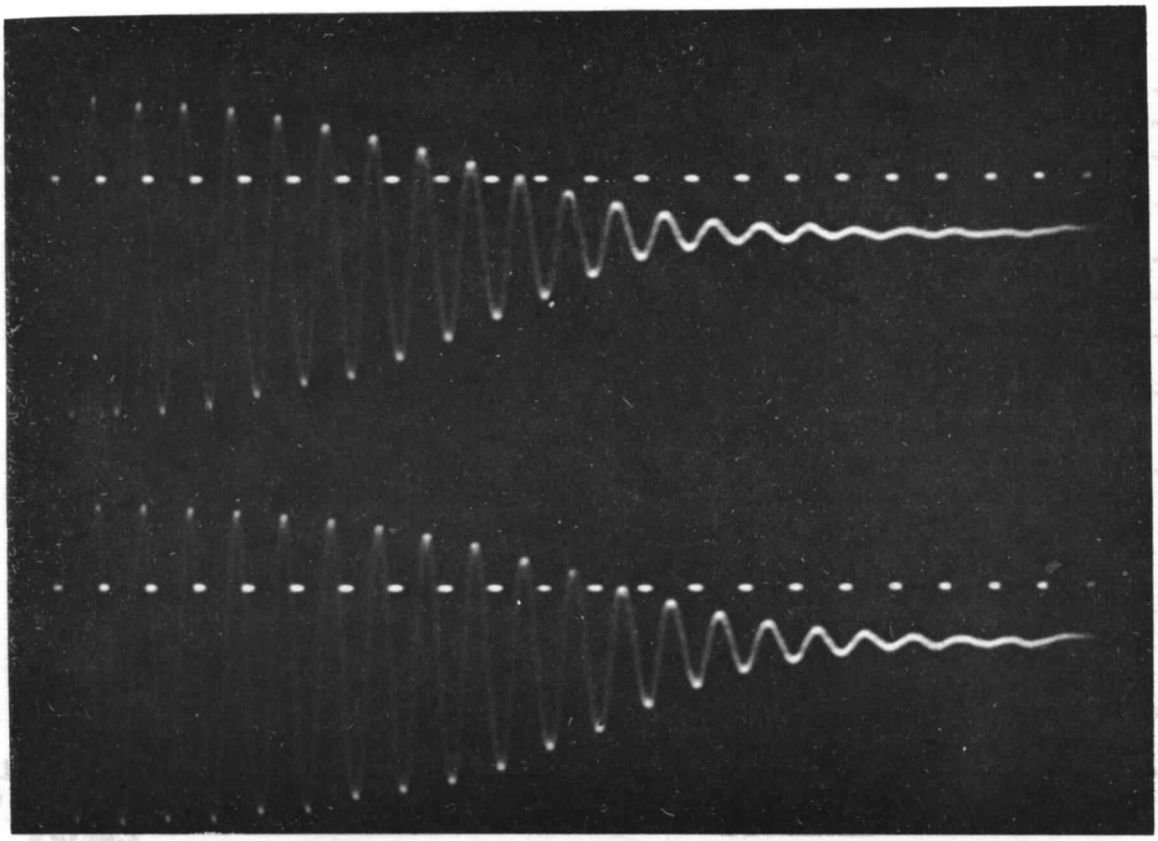

FIG. 4. Two original records showing the variation of flap angle with time.

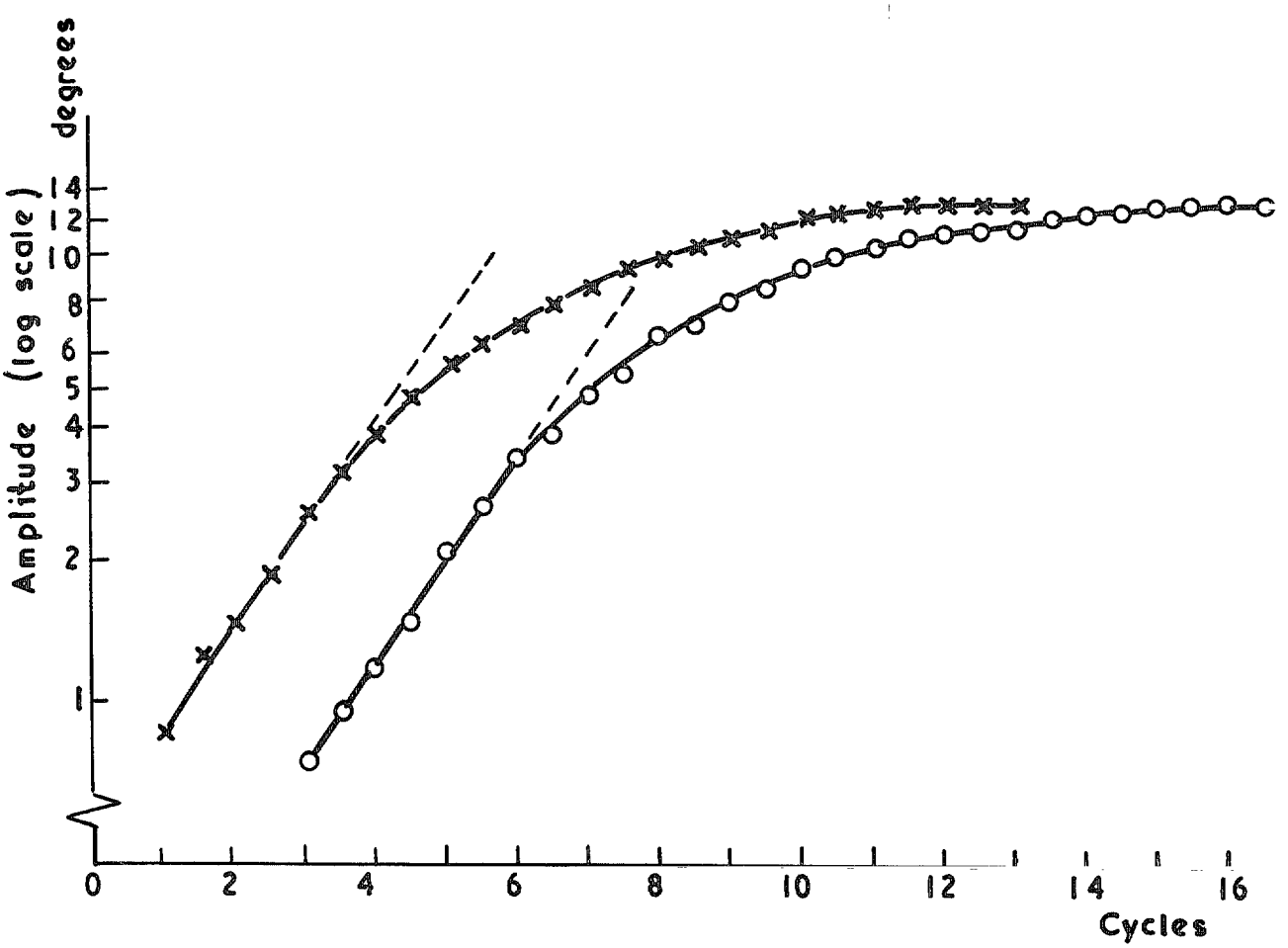

FIG. 5. Typical growth of flap angle amplitude (2 records corresponding to Fig. 4, $M=0{\cdot}78$, $H_0=10{\cdot}5\times10^4$ N/m^2 $f=103{\cdot}5$ c/s).

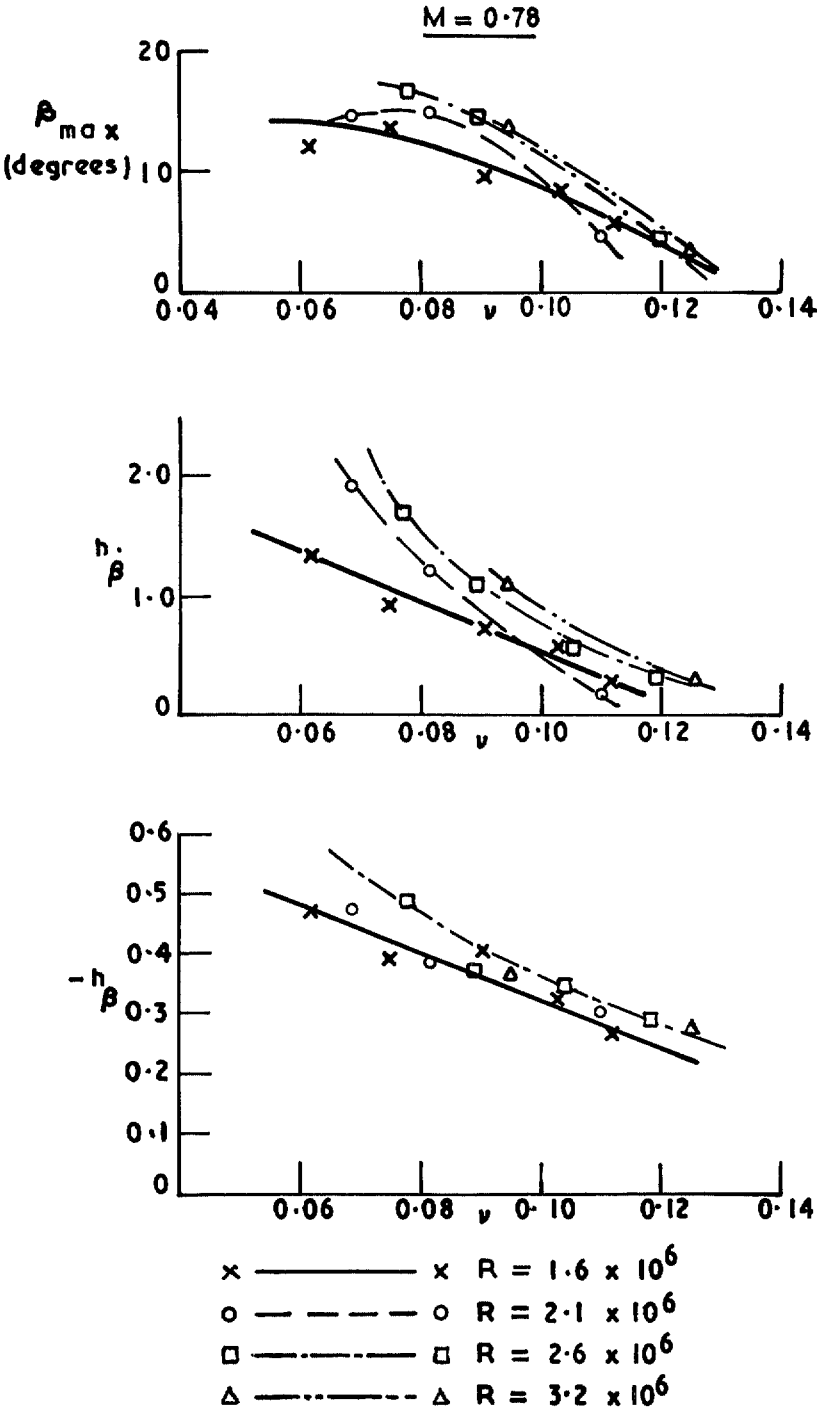

FIG. 6. Variation of the limit cycle amplitude, the stiffness and the damping hinge-moment derivatives, with frequency parameter and Reynolds number at a Mach number of 0·78.

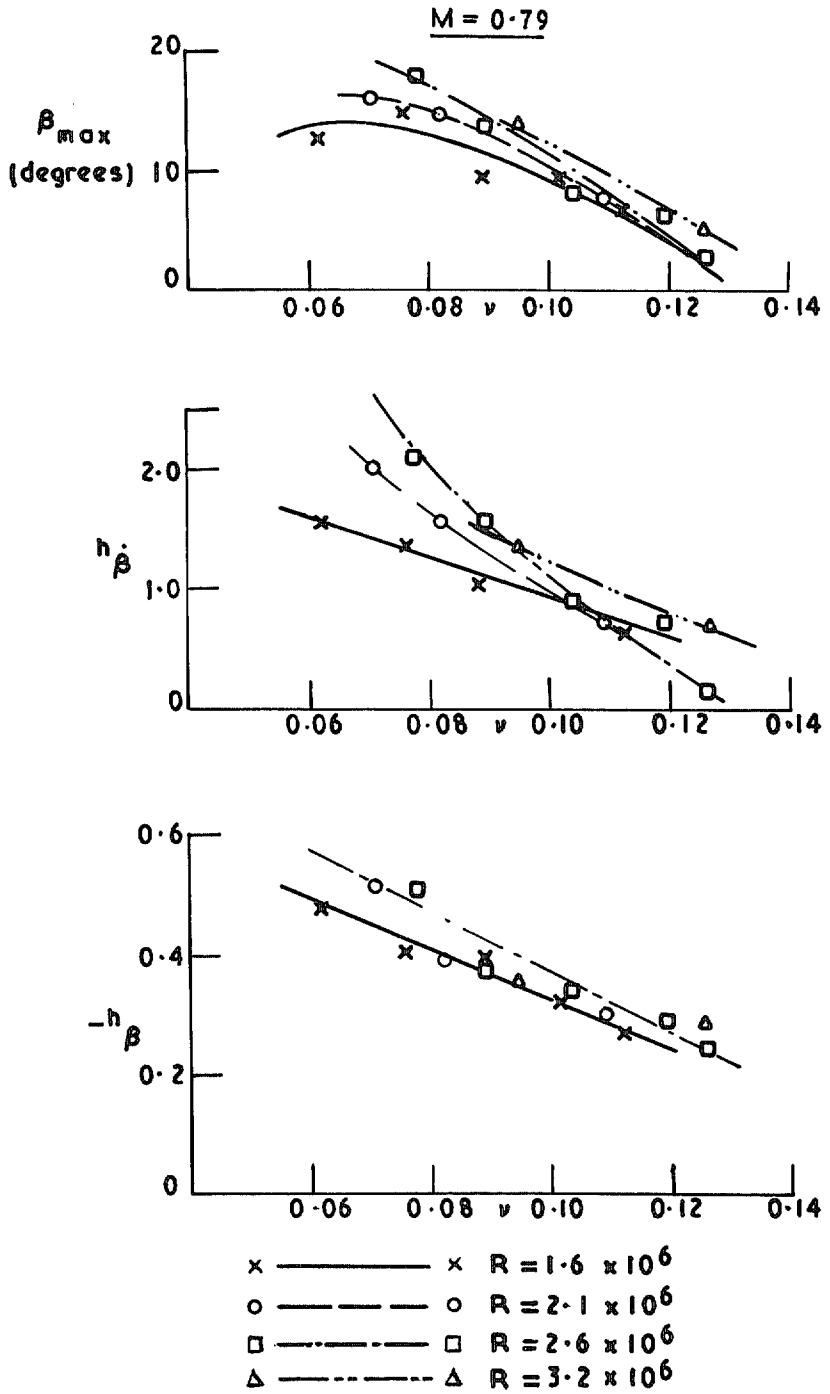

FIG. 7. Variation of the limit cycle amplitude, the stiffness and the damping hinge-moment derivatives, with frequency parameter and Reynolds number at a Mach number of 0·79.

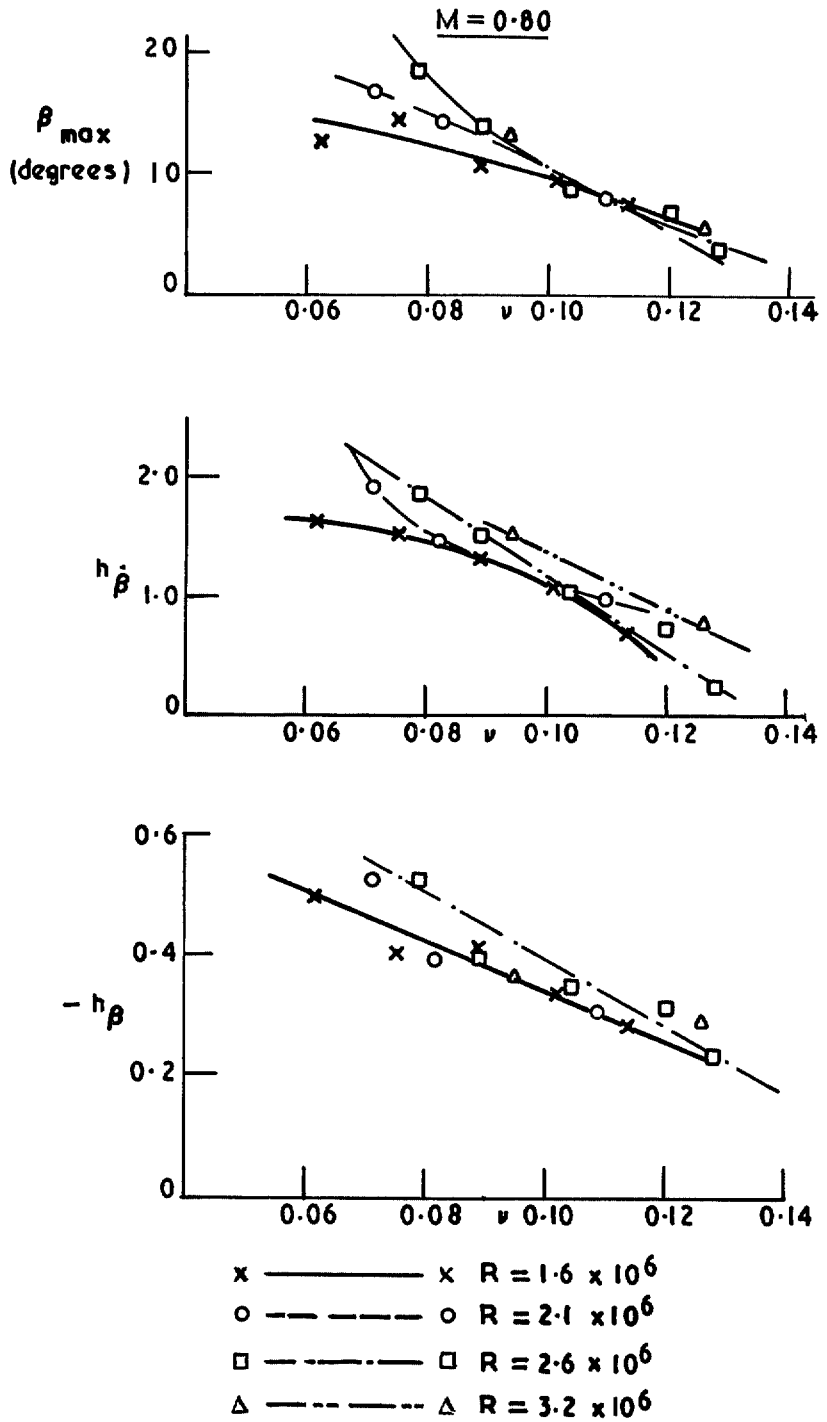

FIG. 8. Variation of the limit cycle amplitude, the stiffness and the damping hinge-moment derivatives, with frequency parameter and Reynolds number at a Mach number of 0·80.

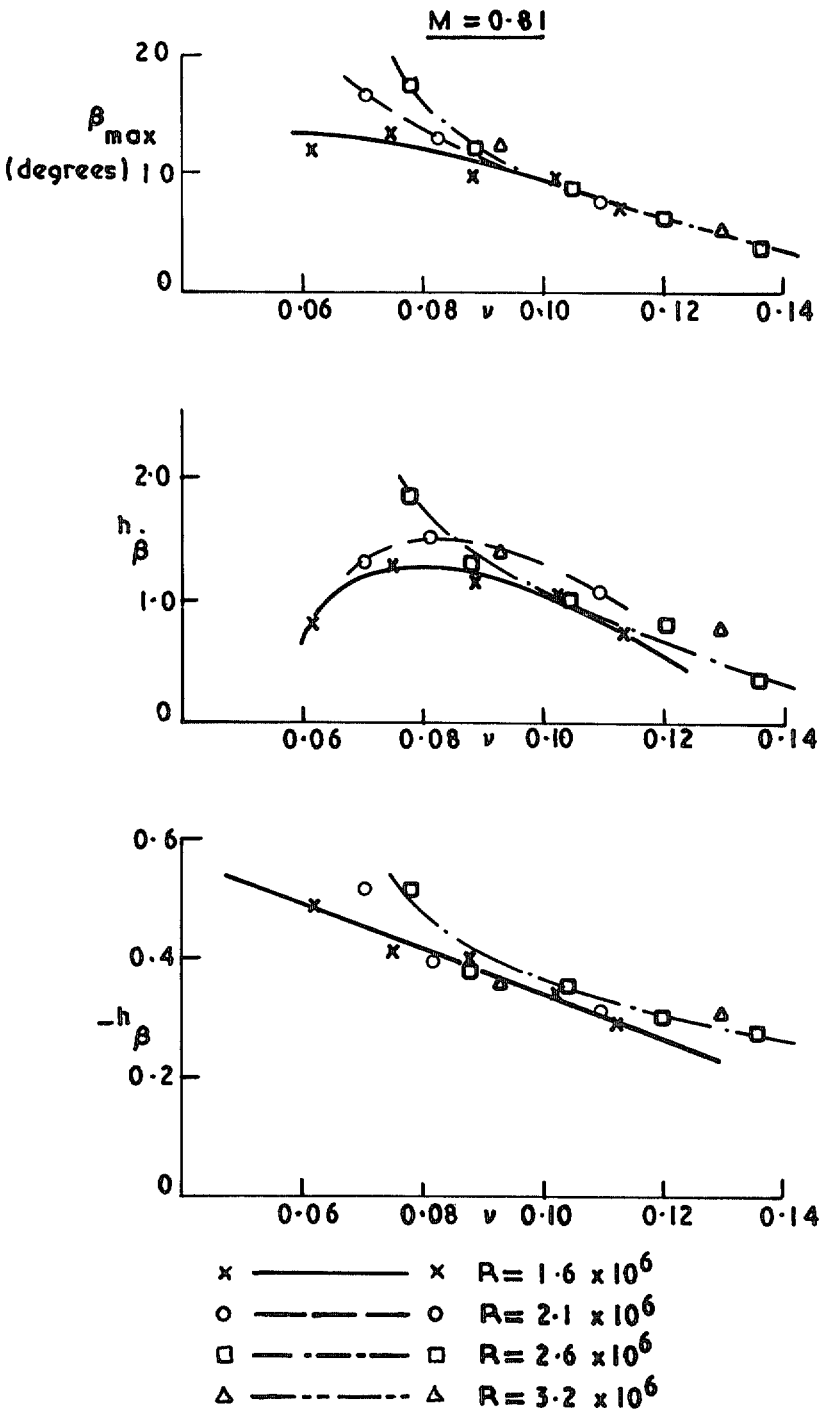

FIG. 9. Variation of the limit cycle amplitude, the stiffness and the damping hinge-moment derivatives, with frequency parameter and Reynolds number at a Mach number of 0·81.

Printed in Wales for Her Majesty's Stationery Office by Allens Printers (Wales) Limited
Dd. 502110 K.5. 5/72

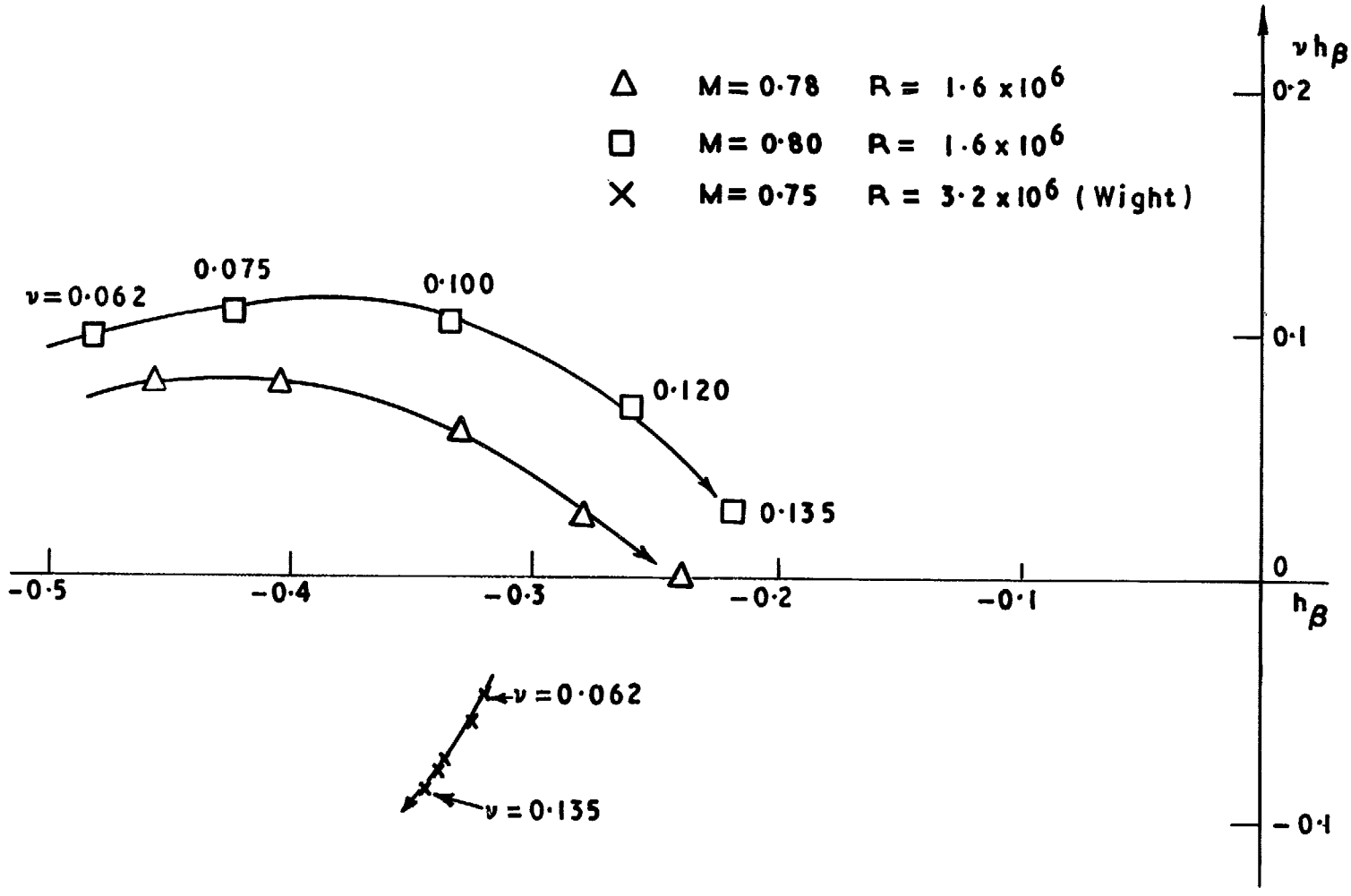

FIG. 10. Vectorial representation of the variation of the unsteady hinge moment with frequency.

HER MAJESTY'S STATIONERY OFFICE
Government Bookshops
49 High Holborn, London WC1V 6HB
13a Castle Street, Edinburgh EH2 3AR
109 St Mary Street, Cardiff CF1 1JW
Brazennose Street, Manchester M60 8AS
50 Fairfax Street, Bristol BS1 3DE
258 Broad Street, Birmingham B1 2HE
80 Chichester Street, Belfast BT1 4JY
Government publications are also available through booksellers

R. & M. No. 3702
SBN 11 470502 X